Hydrological Processes

WILEY

RESEARCH ARTICLE OPEN ACCESS

Quantifying Hydraulic Geometry and Whitewater Coverage for Steep Proglacial Streams to Support Process-Based Stream Temperature Modelling

A. L. Dufficy[1,2] | B. C. Eaton[2,3] | R. D. Moore[2]

[1]Northwest Hydraulic Consultants Ltd., Seattle, Washington, USA | [2]Department of Geography, The University of British Columbia, Vancouver, British Columbia, Canada | [3]BGC Engineering Inc., Vancouver, British Columbia, Canada

Correspondence: R. D. Moore (dan.moore@ubc.ca)

Received: 3 June 2024 | **Revised:** 30 September 2024 | **Accepted:** 5 November 2024

Funding: This work was supported by Natural Sciences and Engineering Research Council of Canada and University of British Columbia Faculty of Arts.

Keywords: breakthrough curve | drone | hydraulic geometry | photogrammetry | proglacial stream | salt injection | structure from motion | whitewater

ABSTRACT

At-a-station hydraulic geometry (AASHG) relationships describe the dependence of a river's width, mean depth and mean velocity on discharge at a given location, and are typically modelled as power-law functions. They are often used when modelling stream temperature under unsteady flow conditions. Deriving AASHG relationships is challenging for steep proglacial streams due to the combination of complex morphology and velocity distributions, and rapidly varying flow. The objective of this study was to combine tracer injections with drone-based photogrammetry to derive AASHG relationships for a steep proglacial channel and to quantify whitewater coverage and its relationship with discharge to support process-based stream temperature modelling. Velocity–discharge and width–discharge relationships were reasonably well characterised using power-law functions, but varied amongst sub-reaches. Whitewater coverage as a fraction of total stream surface area generally exceeded 50% for the range of flows sampled, and exhibited a statistically significant positive relationship with discharge, which varied amongst sub-reaches. For the range of flows captured during drone flights, the relationship could be represented by a linear function. However, an asymptotic model would be required to extend the relationship to higher flows. The magnitude of whitewater coverage indicates that the albedo of the stream should be substantially higher than values typically used in stream temperature models, and the relationship with discharge means that ongoing glacier retreat, and the associated reduction in summer discharge, should result in lower albedo and higher downstream warming rates, reinforcing the effects of decreasing velocity and mean depth as flows decline.

1 | Introduction

Stream temperature is broadly considered the 'master variable' in aquatic ecosystems, and is particularly important in relation to thermal habitat suitability for a range of aquatic species (Barbarossa et al. 2021; Eaton and Scheller 1996; Parkinson et al. 2016). During periods of warm, dry weather in summer, rivers without glacier-melt contributions tend to experience low flows and elevated temperatures, which can be deleterious for cold- and cool-water species such as salmonids (Iacarella et al. 2024; Johnson et al. 2024; Nelitz, MacIsaac, and Peterman 2007). For glacier-fed rivers, increased glacier melt under these weather conditions helps to maintain streamflow and reduce stream temperature increases, and thus maintains their habitat suitability (Fleming 2005; Moore et al. 2009; Pitman and Moore 2021).

Mountain glaciers in most regions of the world are currently retreating and are projected to continue retreating, or even disappear, over the coming decades (Clarke et al. 2015; Zemp et al. 2019). Whilst some rivers may experience temporary increases in streamflow due to increased glacier mass loss, continued retreat will ultimately result in reduced summer flows (e.g. Frans et al. 2018; Huss and Hock 2018). Reductions in summer flow should also be accompanied by higher summer temperatures, with potentially negative impacts on cool- and cold-water fish (Moore et al. 2009). There is a growing need for predictive tools to make projections of future streamflow and temperature conditions for future climate and glacier scenarios (Weller, Moore, and Iacarella 2023).

Whilst empirical models have been used to make projections of the effects of both climate and glacier change on stream temperature (Weller, Moore, and Iacarella 2023), they are based on historical relationships that may not remain valid under changing climatic or land-cover conditions (Arismendi et al. 2014; Leach and Moore 2019). An alternative is to use process-based models, which can be used to assess stream thermal sensitivity to climate and land-cover change both separately and in combination (e.g. Chen et al. 1998; Fullerton et al. 2022; MacDonald, Boon, and Byrne 2014; St-Hilaire et al. 2000; Sun et al. 2015; van Vliet et al. 2012). Process-based stream temperature models solve the water and energy budgets through time at multiple locations along the stream or river network. Solving Eulerian expressions of the stream energy budget requires that the dependence of stream cross-sectional area and surface width on discharge be known (e.g. Glose, Lautz, and Baker 2017). The heat budget equation has also been solved using a Lagrangian or semi-Lagrangian frame of reference, which requires specifying the discharge-dependence of velocity and at least one of cross-sectional area, surface width or depth (e.g. Garner et al. 2014; Yearsley 2009). Accounting for these dependencies on discharge is particularly important for glacier-fed streams and rivers, which typically exhibit substantial diel fluctuations in discharge, especially in late summer, when stream temperatures reach seasonal peaks (Baker et al. 2018).

Most stream temperature models use a one-dimensional representation of the channel network (Dugdale, Hannah, and Malcolm 2017), and two main approaches have been used to quantify the dependence of hydraulic parameters (width, depth, velocity) on discharge for stream temperature modelling under unsteady flow. One is to assume an idealised channel geometry (e.g. rectangular, triangular, parabolic, trapezoidal) and a roughness parameter (e.g. Manning's n), and then to generate hydraulic parameters as a function of discharge as part of the model solution. This approach has been used, for example, by Cardenas et al. (2014), Glose, Lautz, and Baker (2017) and Buahin, Horsburgh, and Neilson (2019). This approach may not work well for steep streams, in part because their complex morphologies may deviate substantially from the idealised cross-sectional forms typically assumed. In addition, flow resistance decreases quickly with increasing flow depths (e.g. Dingman and Afshari 2018; Ferguson 1986; Ferguson 2007), such that velocity increases faster with increasing depth than predicted by the Manning's or Chezy equations.

An alternative approach is to use at-a-station hydraulic geometry (AASHG) relationships, which are typically modelled as empirically derived power-law functions (Leopold and Maddock 1953). They have been applied in a broad range of applications, such as characterising the dependence of fish habitat on stream discharge (McParland, Eaton, and Rosenfeld 2014; Saraeva and Hardy 2009) and simulating the routing of water down channel networks for modelling contaminant transport (Gu 1998). They have been used in stream temperature models for unsteady flow conditions using both Eulerian and Lagrangian frames of reference (Chikita et al. 2010; Foreman et al. 1997; Garner et al. 2014; Yearsley 2009).

At locations with relatively smooth beds, hydraulic geometry relationships can be generated from measurements of depth and velocity across a channel – for example, using a current meter or acoustic Doppler current profiler. However, these approaches are challenging to employ for steeper channels dominated by step-pool or boulder-cascade units, which have complex bed morphologies and velocity profiles. An alternative approach is to estimate reach-averaged velocities from analysis of tracer breakthrough curves (BTC) (David et al. 2010; Lee and Ferguson 2002; Magnusson, Jonas, and Kirchner 2012; Schneider et al. 2015).

Under conditions with relatively steady flow, surface width can be sampled in the field at multiple locations to compute a reach-scale mean (Lee and Ferguson 2002). However, under unsteady flow conditions, it may be challenging to acquire a robust sample of surface widths if discharge changes substantially over the time interval required to conduct the field surveys. Magnusson, Jonas, and Kirchner (2012) back-calculated reach-average surface width from stream temperature using a Lagrangian energy-balance approach, but that approach is subject to uncertainty associated with the assumed value of stream albedo and the exchange coefficients for sensible and latent heat transfer, as well as heat exchange terms not included in the energy-balance model (Leach et al. 2023; McMahon and Moore 2017; Szeitz and Moore 2020).

Over the last decade, drone-based remote sensing has become increasingly popular for characterising stream characteristics such as surface temperature and riparian vegetation (Dugdale et al. 2019; Dugdale, Malcolm, and Hannah 2019; Fuller et al. 2021), but applications to quantify width–discharge relationships appear to be limited to date. Cardenas et al. (2014) used ground-based thermal imaging not only to characterise stream temperature, but also to determine wetted width for stream temperature modelling. However, their model set-up assumed a rectangular cross-section and thus did not accommodate temporal variability in wetted width. King and Neilson (2019) successfully used drone-based imagery acquired for a range of discharges to derive width–discharge relationships for modelling temperature dynamics for a relatively low-gradient cobble-bed Arctic river. To the authors' knowledge, no studies have used drone-based imagery to derive width–discharge relationships for proglacial streams subject to strong diel fluctuations in width and streamflow.

Stream surface albedo is a key parameter for stream temperature modelling given that solar radiation is typically the

dominant surface energy input on summer days in environments that lack substantial shading by riparian vegetation (Dugdale et al. 2018; Khamis et al. 2015; King and Neilson 2019; Moore et al. 2005). Many modelling studies assumed a constant value for stream surface albedo, typically 0.03 or 0.05 (Caissie, Satish, and El-Jabi 2007; Garner et al. 2014; Magnusson, Jonas, and Kirchner 2012), or have used published equations that relate albedo to angle of incidence, cloud cover and/or other variables (Boyd and Kasper 2003; Meier et al. 2003). Others have used field measurements of incident and reflected solar radiation to specify albedo (Chikita et al. 2010; King and Neilson 2019; Leach and Moore 2010). Field-determined albedo values for non-turbid flatwater conditions have ranged from 0.03 to 0.12, with higher values corresponding to higher solar incidence angles (King and Neilson 2019; Leach and Moore 2010; McMahon and Moore 2017). However, the albedo of mountain streams with high turbidity and/or whitewater can be substantially higher (McMahon and Moore 2017). Chikita et al. (2010) reported a value of 0.1 for a turbid proglacial river, and Richards and Moore (2011) reported that the albedo of a steep, boulder-dominated proglacial stream varied with discharge, from about 0.1 at lower flows to about 0.4 at higher flows, reflecting the effect of increasing extent and magnitude of aeration at higher discharges. Chikita et al. (2010), Richards and Moore (2011) and McMahon and Moore (2017) all sampled albedo over limited areas of the stream surface; to the authors' knowledge, no studies have attempted to generate reach-scale estimates of albedo or whitewater coverage for steep channels with substantial aeration.

This study was conducted as part of a broader project focused on process-based modelling of proglacial stream temperature dynamics. The objective of this study is to use a combination of tracer injections and drone-based photogrammetry to quantify hydraulic geometry relationships and to quantify whitewater coverage and its dependence on discharge along a steep, proglacial stream channel.

2 | Methods

2.1 | Study Site

This study was conducted on a glacier-fed tributary of the upper Bridge River, unofficially known as South Creek (Ryder 1991), located in the southern Coast Mountains of British Columbia (Figure 1). South Creek is currently incising into a lateral moraine that once impounded a glacial lake within the creek's headwater valley (Figure 2). The erosion of the moraine occurred during multiple outburst floods between 1935 and 1970 (Ryder 1991). Based on comparison of historic aerial photographs, an avulsion took place in the 1980s that diverted the lower 500 m of the stream into its current channel path.

The study focused on a 945-m-long section of South Creek, with the upper boundary located at the breached moraine. At the upstream boundary, the catchment area is 20% glacierised. The hydrologic regime is dominated by spring–summer meltwater, initially dominated by seasonal snowmelt and transitioning to glacier melt later in the summer. Summer discharges generally range from about 0.5 to 4 $m^3 s^{-1}$ (Bird et al. 2022).

The reach was chosen because it has no tributary confluences and only a minor increase in contributing area along its length, and thus was expected to have only a minor influence from lateral inflows: the contributing area is 17.5 km^2 at the upstream boundary and 17.8 km^2 at the downstream extent. This criterion was important in the broader context of energy-balance modelling, where the focus was on surface energy exchanges, and the desire was to minimise the influence of advective heat inputs. In addition, we had previous experience in stream gauging along the reach, including an understanding of mixing characteristics (Bird et al. 2022; Richardson, Moore, and Zimmermann 2017).

The elevation of the study reach ranges from 1500 m to 1400 m above sea level (m.a.s.l.). The bed and banks of the study reach are composed almost entirely of granitic morainal till and are almost completely unvegetated. Cobbles and boulders dominate the clast size portion of the bed. The channel is dominated by step-pool and cascade morphologies.

The 945-m-long study reach was divided into four sub-reaches with differing morphologies (Table 1, Figure 3). The boundaries were based primarily on changes in channel gradient and morphology, but were adjusted based on the criterion of achieving complete tracer mixing at the lower boundary for the discharge measurements by salt dilution. The upper-most sub-reaches, R3 and R4, have the highest slopes as they continue to incise into the lateral moraine. These sub-reaches are characterised by mainly step-pool and cascade morphologies. Sub-reaches R2 and R1 have lower gradients. Based on a visible change in morphology, sub-reach R1 was separated into lower and upper R1 sections for determining the width–discharge relationship. Access to the stream from the field camp was from the east, and it was not safe to cross the stream except for a location upstream of the breached moraine. Therefore, manual field measurements were made from the right (east) bank of the stream, and field operations on the west side of the stream were restricted to deploying and removing markers for ground control points.

The study site is remote and was accessed by float plane from Tyaughton Lake, located about 50 km east of the study site. Four field campaigns were conducted during summer 2017, spanning the following dates: July 3–7, July 22–30, August 15–23 and September 6–10.

2.2 | Meteorological Data

A weather station was set up on a terrace about 50 m east of South Creek at an elevation of 1410 m, at a site with minor topographic shading. Among other variables, the station monitored solar radiation using a Kipp and Zonen CM3 pyranometer (stated accuracy ± 10%), air temperature using a shielded Rotronic HC-S3 sensor (stated accuracy ± 0.2°C) and rainfall with a TX Electronics TR525M tipping bucket gauge. All instruments were scanned and data recorded using a Campbell Scientific CR10x data logger. Solar radiation and air temperature were scanned every 10 s, and means were computed and stored every 10 min. Total rainfall was recorded every 10 min. For this study, the 10-min-resolution data were aggregated to generate daily minimum, mean and maximum air temperature (°C), total daily solar radiation (MJ $m^{-2} day^{-1}$) and total daily rainfall (mm).

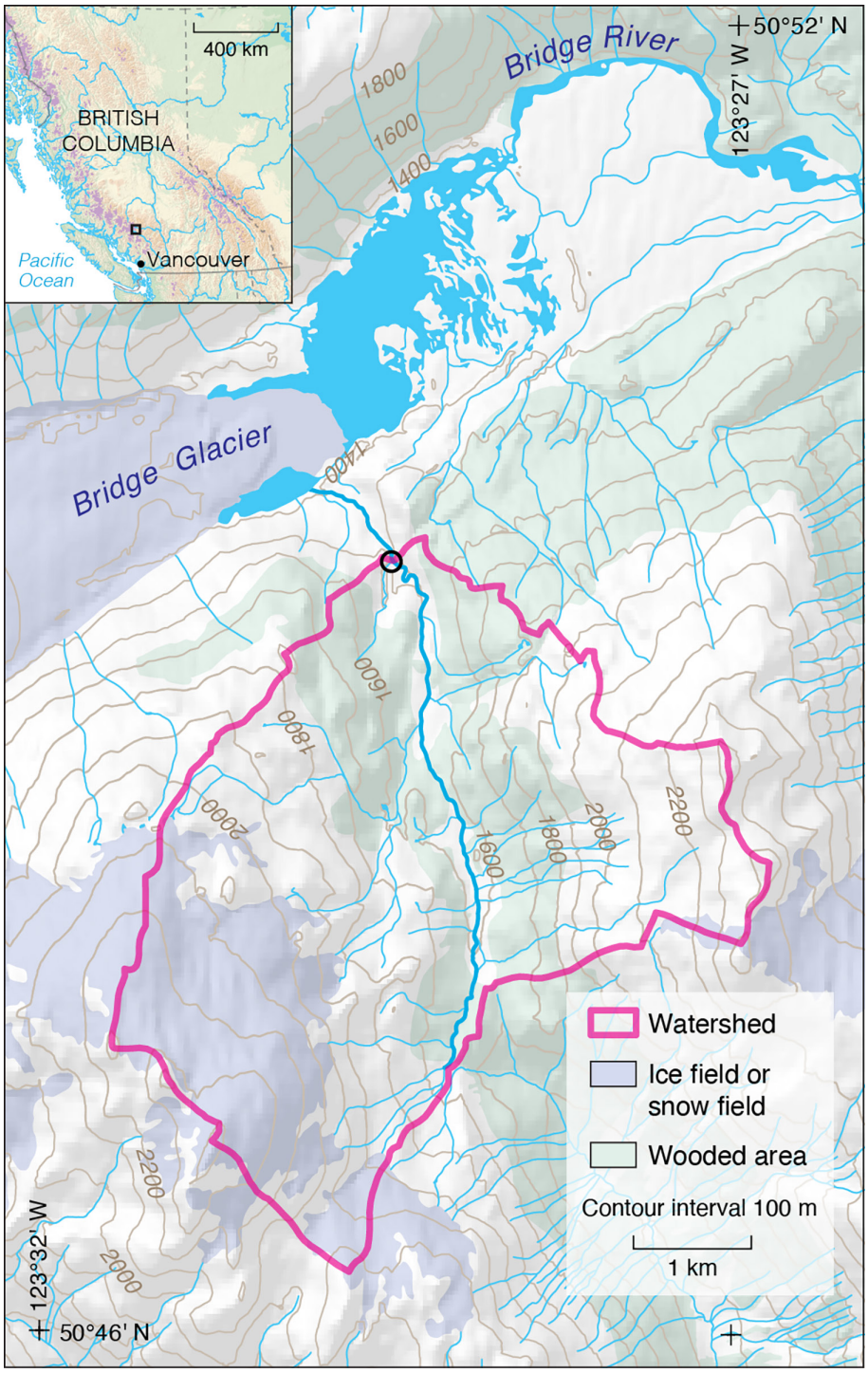

FIGURE 1 | Map of South Creek and its catchment at the upper end of the study reach. The circle indicates the upper boundary of the study reach.

2.3 | Discharge Measurements

Streamflow was measured at the lower end of each sub-reach by dilution gauging using the mass balance method (Richardson, Moore, and Zimmermann 2017). A known amount of NaCl (usually a 2 kg box) was injected upstream of the lower end of each sub-reach. In order to promote rapid dissolution and lateral mixing of the tracer, salt was injected upstream of flow constrictions or in highly turbulent areas. The boxes were weighed to the nearest 0.1 kg before (with salt) and after (empty) injection to reduce the uncertainty in the injected mass to under 0.1%.

Electrical conductivity was measured at the lower end of each sub-reach during injection trials using a WTW LF-340 meter, with temperature compensation applied using a non-linear function programmed into the meter. The conductivity meters output a voltage that is equivalent to the temperature-compensated EC, which was scanned every 1 s and the average recorded every 5 s by a Campbell Scientific CR510 data logger. Injections were repeated 10–13 times throughout the summer in each of the four sub-reaches in order to capture a range of flows over the field season. Timing of the salt wave relative to the time of injection was also recorded to allow calculation of travel times.

FIGURE 2 | Oblique photograph of study reach.

TABLE 1 | Characteristics of the study sub-reaches.

Sub-reach	Slope ($m\,m^{-1}$)	Length (m)	Morphology
1	0.066	250	Step-pool
2	0.076	240	Step-pool
3	0.160	330	Cascade and step-pool
4	0.110	125	Cascade and step-pool

Discharge was computed as

$$Q = \frac{M}{\Delta t \sum C(t_i)} \tag{1}$$

where Q is discharge ($m^3\,s^{-1}$), M is the mass of salt injected (kg), $C(t_i)$ is the concentration of the injected salt observed at time t_i since injection (s), Δt is the recording interval (s) and the summation covers the period for which $C(t_i) > 0$. The concentration of injected salt was computed as

$$C(t_i) = \mathrm{CF}_T\left[\mathrm{EC}(t_i) - \mathrm{EC}_{\mathrm{bg}}\right] \tag{2}$$

where $\mathrm{EC}(t_i)$ is the electrical conductivity of the stream water recorded at time t_i ($\mu S\,cm^{-1}$), $\mathrm{EC}_{\mathrm{bg}}$ is the background electrical conductivity ($\mu S\,cm^{-1}$) and CF_T is a calibration factor related to the molar conductivity of NaCl, determined empirically in the field using the procedure described by Richardson, Moore, and Zimmermann (2017). Glass pipettes and a volumetric flask were used to minimise uncertainty (Richardson et al. 2017).

2.4 | Stream Velocity

The mixing-reach-averaged velocity for each salt injection was computed as

$$v = \frac{L_{\mathrm{m}}}{\tau_{\mathrm{hm}}} \tag{3}$$

where v is mean velocity ($m\,s^{-1}$), L_{m} is the length of the mixing reach between the injection point and the EC probe (m) and τ_{hm} is the harmonic mean velocity (Zimmermann 2010). The harmonic mean travel time was computed as

$$\tau_{\mathrm{hm}} = \frac{\sum C(t_i)}{\sum \left[C(t_i)/t_i\right]} \tag{4}$$

where the summations cover the period for which $C(t_i) > 0$.

2.5 | Stage Measurement

Continuous water level measurements were recorded in three locations using Onset U20 pressure transducers, at distances of 0, 565 and 810 m from the upstream end of the study reach. The 0-m logger was located in a pool formed just upstream of the breached moraine, and the two lower loggers were located in pools that were judged to have a reasonably effective hydraulic connection to the main flow at the time of installation.

Stage measurements were processed by subtracting barometric pressure, measured with an aerially exposed transducer located at the upstream end of the study section, from the raw pressure data. Shifts in the recorded stage occurred when the transducers were removed from the stream for downloading and then replaced in the stream. These shifts were computed based on the recorded stage before and after downloading and shift corrections were applied to ensure a consistent time series.

2.6 | Rating Curves

Discharge measurements were paired with stage values from the closest upstream pressure transducer; the upstream stage record was used for sub-reaches 4 and 3 whilst the mid-reach record was used for sub-reaches 2 and 1. Stage values were linearly interpolated from the sampled time series for the time associated with the peak of the salt BTC. The initial intention was

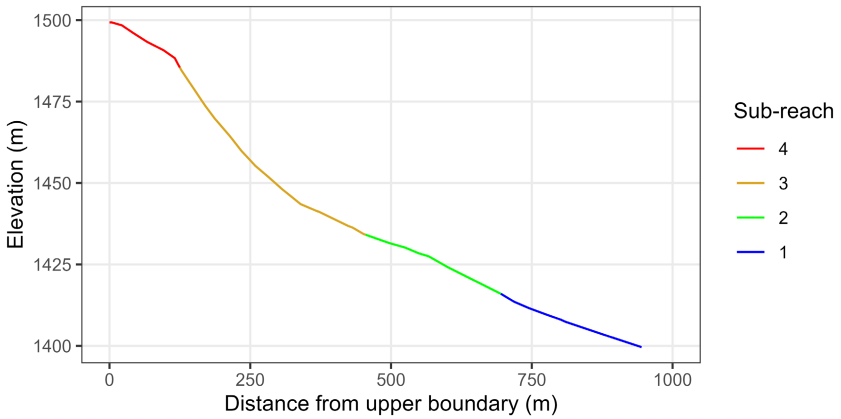

FIGURE 3 | Long profile of the study reach showing sub-reaches. Elevation data are from the Canadian DEM, which can be accessed via https://maps.canada.ca/czs/index-en.html.

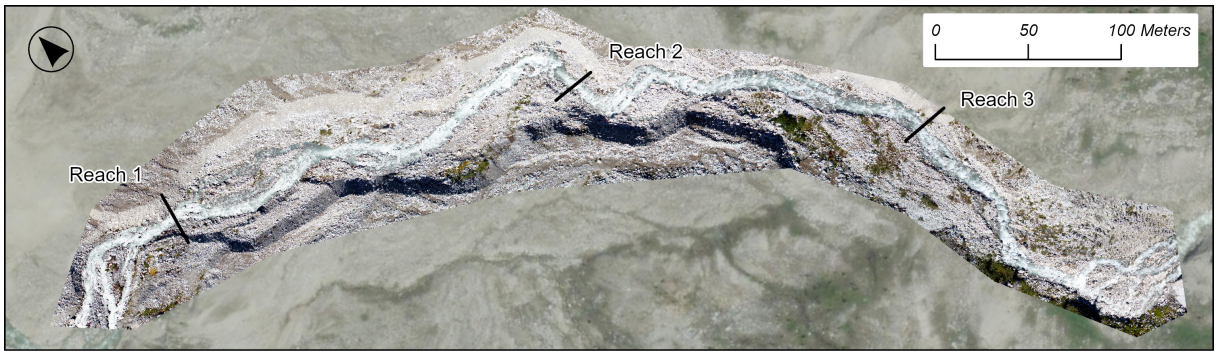

FIGURE 4 | A portion of an orthophoto showing the lower three sub-reaches taken on 20 August 2017. The black lines indicate the lower boundaries of the sub-reaches. Flow is from right to left.

to derive separate rating curves for each sub-reach. However, after omitting salt dilution measurements that were not deemed reliable – for example due to the conductivity not returning to background after the salt wave passage – we combined measurements for sub-reaches 1 and 2, and for sub-reaches 3 and 4, to increase the sample size and range of measurements for fitting the rating curves.

Separate rating curves were constructed for sub-reaches 1/2 and 3/4 using a power-law model of the following form:

$$Q = \alpha\left(h - h_0\right)^{\beta} + e \tag{5}$$

where Q is measured discharge ($m^3 s^{-1}$), h is the stage (m) extracted from the closest pressure transducer corresponding to the time of the discharge measurement, α, h_0 and β are estimated parameters and e is the residual. Rating curves were fit via non-linear least-squares regression using the *nls* function in R. The observations were weighted according to $\hat{y}^{-2}$, where $\hat{y}$ is the predicted value for a given observation. This weighting scheme is consistent with proportional errors (Moore 2024), which is a more realistic assumption than constant errors for discharge measurements. The solution was fit iteratively, with weights being recalculated after each iteration and then used in the next iteration. Prediction limits were computed using the *predFit* function from the *investr* R package (Greenwell and Kabban 2014) for a confidence level of 0.9.

2.7 | Determination of Surface Width

For the lower three sub-reaches, width was measured remotely using drone-based orthomosaic images taken from a DJI Phantom 4 quadcopter drone (see Figure 4 for an example). The drone flights, 11 in total, did not extend over sub-reach 4 due to concerns about flying the drone in the narrow canyon formed by the breached moraine. South Creek is otherwise well suited to mapping by structure from motion (SfM) photogrammetry due to the lack of vegetation near the stream. The drone was flown at a constant height of 50 m above the take-off location, which was located in the middle of sub-reach 2. Drone speed was also kept constant.

Prior to the aerial surveys, a total of 25 ground control points was established on both sides of the stream and surveyed using a total station for use in georeferencing the drone imagery. Three total station set-ups were used to complete the survey, with each station location surveyed from subsequent set-ups in order to ensure accuracy in the results and account for the compounded error acquired when moving the instrument. Overlapping images and alternating camera angles reduced artificial surface curvature and optimised the 3D accuracy of a given feature. Unfortunately, the highest flows were not captured due to drone charging difficulties in the first field campaign (July 3–7), when the highest discharges occurred.

Following completion of the field campaigns, orthomosaic images and DEMs were created in AgiSoft Photoscan Version 1.2

for each flight. The first step was to create a dense point cloud using the 'ULTRA HIGH' setting. The ground control points were then linked to the point cloud, after which the point cloud was re-optimised using the ground control points. Dense clouds and mesh were then created. The dense clouds were processed using the 'HIGH' option for the 'dense cloud quality parameter', followed by creation of a texture. Finally a DEM was created from the dense cloud and an orthomosaic was created from the DEM and texture. Vertical accuracy of the DEMs ranged between 5 and 10 cm after comparing the coordinates of the control points from the total station to DEM-derived elevations. The horizontal resolution of the DEM was 3 cm.

Channel dimensions were determined by extracting surface area information obtained from aerial imagery analysis using methods and suggestions from a study of braided streams by Javernick, Brasington, and Caruso (2014). Wetted surface width was manually measured every 10 m along the stream from the orthomosaics using the measuring tool in ArcGIS. These values were then averaged for each sub-reach, and the corresponding discharge was extracted from the discharge time series for the sub-reach generated using the stage record and the rating curve. Wetted width was also measured at 25-m intervals along all four sub-reaches using a laser rangefinder, using the waterline on the opposite bank for a target. At locations where some of the flow was carried by small side channels, these widths were measured using a 30-m tape and added to the width of the main channel.

2.8 | Whitewater Coverage

For the three lower sub-reaches, R1–R3, whitewater coverage was determined manually from the orthomosaic images using the same transects used for determining wetted width by also measuring the width on each transect of non-aerated water. The fraction of the stream surface that exhibited whitewater (f_{ww}) was then computed as

$$f_{ww} = 1 - \frac{\sum_{i=1}^{n} w_{ni}}{\sum_{i=1}^{n} w_i} \tag{6}$$

where w_{ni} is the width of non-aerated water surface in transect i, w_i is the total width at transect i and n is the total number of transects measured in the orthomosaic for each reach.

2.9 | Hydraulic Geometry Relationships

Hydraulic geometry relationships of the following forms were fit to the data:

$$w_s = aQ^b \tag{7}$$

and

$$v = kQ^m \tag{8}$$

where w_s is surface width (m), v is mean velocity ($m\,s^{-1}$), Q is discharge ($m^3\,s^{-1}$) and a, b, k and m are parameters to be estimated. For consistency with the approach used in most previous studies of AASHG, the coefficients in Equations (7) and (8) were estimated by transforming v, w_s and Q by taking their logarithms and applying linear regression. For example, the fitted $v - Q$ relationship can be expressed as

$$\log(v) = b_0 + b_1 \log(Q) + e \tag{9}$$

where b_0 and b_1 are the estimated intercept and slope for the log–log linear relationship, and e is the residual. The coefficient and exponent in the original power-law relationship can be estimated as

$$m = b_1 \tag{10}$$

and

$$k' = \exp(b_0) \tag{11}$$

where k' is the back-transformed estimate of k. The value of k' estimated by back-transformation will be biased (Moore 2024). Here, the non-parametric bias-correction introduced by Duan (1983) was applied, which involves adjusting k' as follows:

$$k = k' n^{-1} \sum \exp(u_i - \hat{u}_i) \tag{12}$$

where u_i is $\log(v_i)$, $\hat{u}_i$ is the predicted value of $\log(v_i)$ from Equation (9) and n is the number of points used to fit the regression.

2.10 | Calculation of Celerity

For kinematic flow, wave celerity c ($m\,s^{-1}$) can be expressed as follows:

$$c = \frac{dQ}{dA} \tag{13}$$

where A is cross-sectional area (m^2). The relationship between cross-sectional area and discharge is often modelled as a power-law function:

$$A = fQ^g \tag{14}$$

By definition, $Q = Av$, so that the following relationships hold due to continuity:

$$f = k^{-1} \tag{15}$$

and

$$g = 1 - m \tag{16}$$

Combining Equations (13), (14), (15) and (16) and re-arranging yields the following expression for celerity:

$$c = \frac{k}{1-m} Q^m \tag{17}$$

Comparison of Equations (8) and (17) indicates that celerity is proportional to velocity, with a constant of proportionality equal to $(1-m)^{-1}$.

3 | Results

3.1 | Weather During the Study Period

The study period was dominated by high pressure systems, as is typical of summer weather in southern British Columbia, which tend to bring clear skies (Moore et al. 2010). Relatively cool conditions occurred in mid-July, with daily maxima generally below 15°C and with rain falling on 5 days, mostly between July 20 and July 22 (Figure 5). The period from July 23 to August 13 was dry with a warming trend, with daily maximum air temperatures rising to about 23°C. Cooler weather resumed August 13, with rain falling on August 13 and August 22–24.

3.2 | Stage and Discharge

The stage records for the upper two loggers were highly correlated (Pearson's $r = 0.97$, $n = 9508$), but stage at the 810-m site had a correlation of $r = -0.11$ ($n = 9390$) with stage at the 0-m site and -0.03 ($n = 9390$) with stage at the 565-m site. Visual examination of the time series indicated that stage at the 810-m site became erratic in mid to late August. Therefore, only stage data from the upper two loggers were used in the analysis, as described in Section 2.

The rating curves were reasonably well defined (Figure 6), and there are no obvious systematic differences in the stage–discharge relationships for sub-reaches 1 and 2 or for 3 and 4. Streamflow time series were reasonably consistent between sub-reaches 1/2 and 3/4 (Figure 7a), although visible differences in the sequences of peaks and troughs suggest the occurrence of flow losses and gains between the lower boundaries of sub-reaches 2 and 3 (Figure 7a). This pattern is more clearly seen in the time series of daily mean discharge (Figure 7b). Discharge for sub-reaches 1/2 was initially higher than for sub-reaches 3/4, indicating gaining conditions. The net inflow appeared to decline through time, with a shift to losing conditions by August 1. A relatively abrupt shift back to gaining conditions occurred around August 20, coincident with a rain event (Figure 5).

3.3 | Velocity and Celerity

Velocity has a linear relationship with discharge when plotted with logarithmic axes, supporting the use of a power-law model (Figure 8). For a given discharge, velocity generally increased from upstream to downstream. The exponents, m, in the fitted power-law relationships ranged from 0.32 to 0.54 (Table 2). The exponent decreased from sub-reach 3 to sub-reach 1, but was lowest in sub-reach 4.

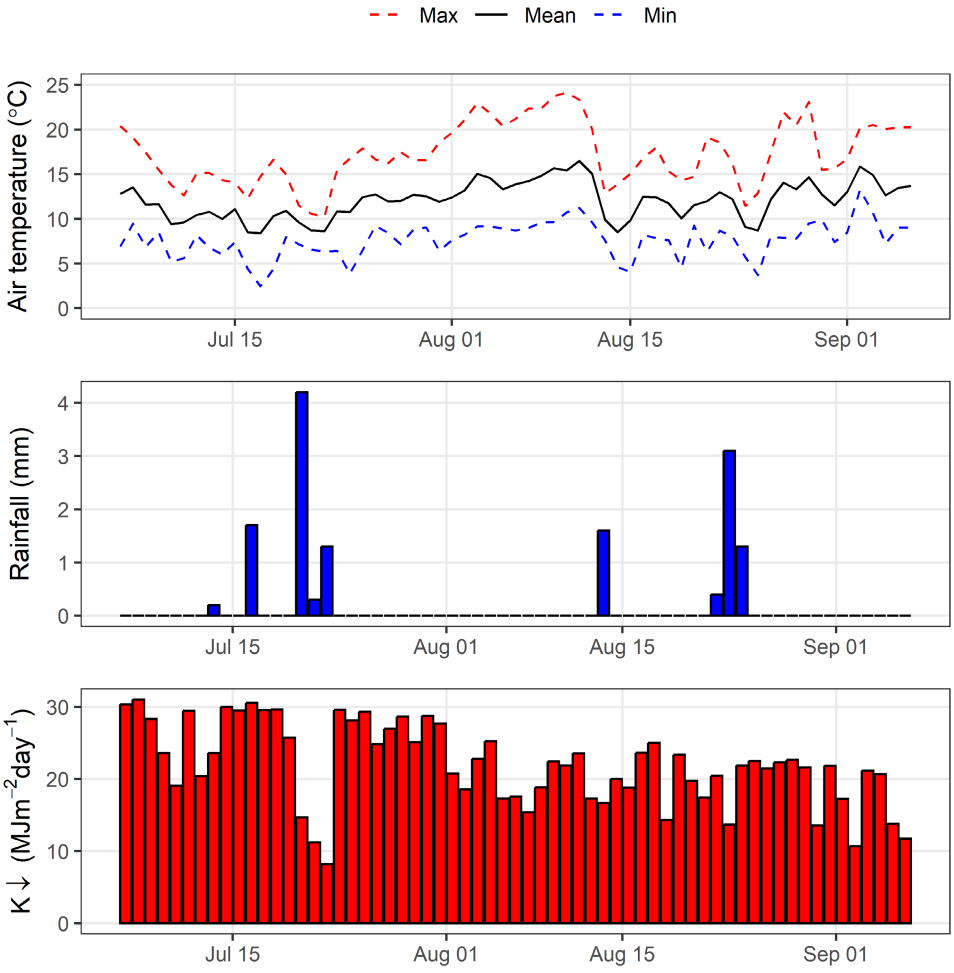

FIGURE 5 | Time series of daily meteorological elements during the study period. $K\downarrow$ is daily total solar radiation.

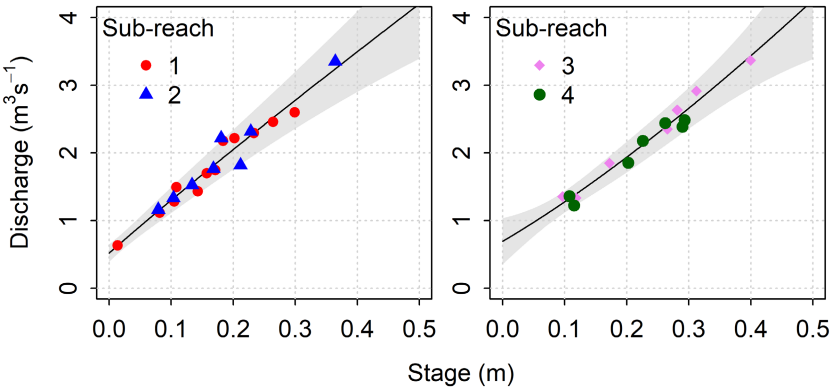

FIGURE 6 | Rating curves for sub-reaches 1 and 2 (left panel) and 3 and 4 (right panel). The grey ribbons are prediction limits for a 90% confidence level, based on proportional errors.

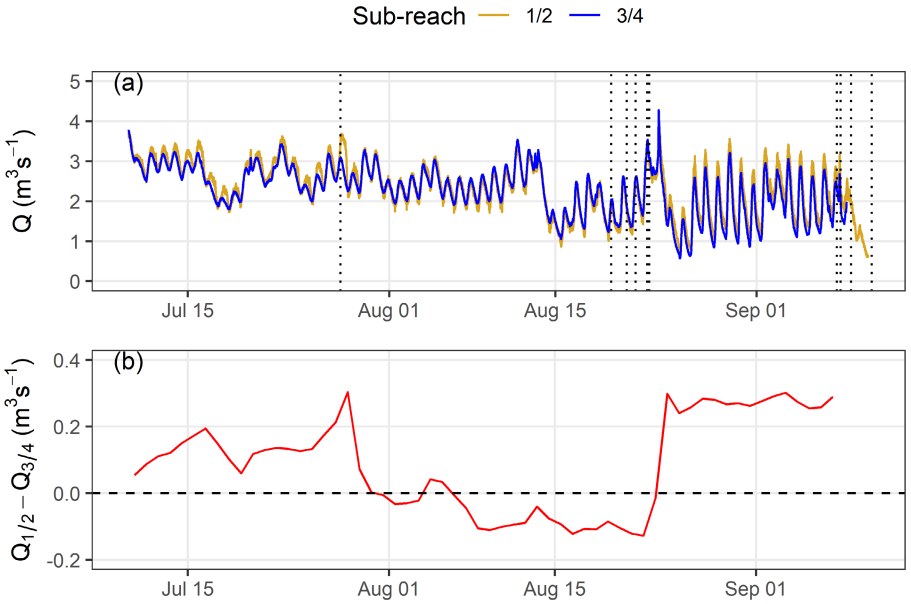

FIGURE 7 | Streamflow time series for sub-reaches 1/2 and 3/4. Panel (a) shows time series of streamflow (Q) with a resolution of 10 min; panel (b) shows the difference in daily mean streamflow between sub-reach 1/2 and sub-reach 3/4. Vertical dotted lines indicate times of drone flights.

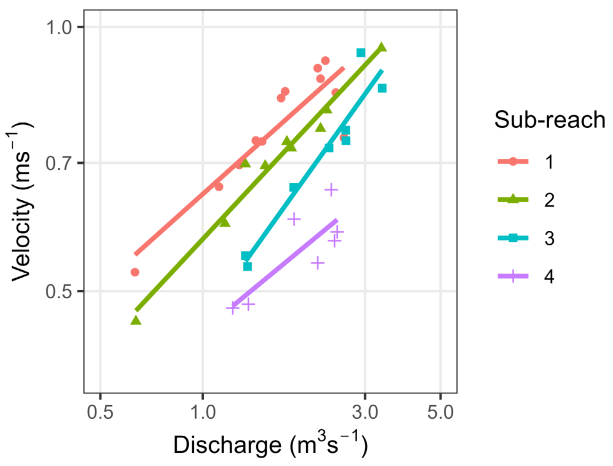

FIGURE 8 | Relationships between mean velocity and discharge, showing the observed values and best-fit lines. Both axes are logarithmic.

Celerities for all sub-reaches were generally greater than 0.5 m s^{-1} (Figure 9). Sub-reach 4 had the lowest celerities. The other three sub-reaches had celerities in excess of 1 m s^{-1} for discharges greater than 1 m^3s^{-1}. Using a nominal celerity of 1 m s^{-1}, the time taken for a given discharge to propagate 500 m downstream (i.e. roughly the distance from the upstream stage record to the lower boundary of sub-reach 3 or from the middle stage record to the lower boundary of sub-reach 1) would be about 8 min, or less than the sampling interval of the stage measurements.

3.4 | Width and Fractional Whitewater Coverage

When plotted on logarithmic axes, width exhibited a roughly linear relationship with discharge, consistent with a power-law model (Figure 10). The exponents in the fitted power-law relationships ranged from 0.16 to 0.38 (Table 3).

TABLE 2 | Estimated parameters in the power-law relationship between velocity and discharge.

Sub-reach	k	m	n
1	0.647	0.348	12
2	0.573	0.416	9
3	0.463	0.542	8
4	0.452	0.320	7

Note: n is the number of data points used to fit the relationship.

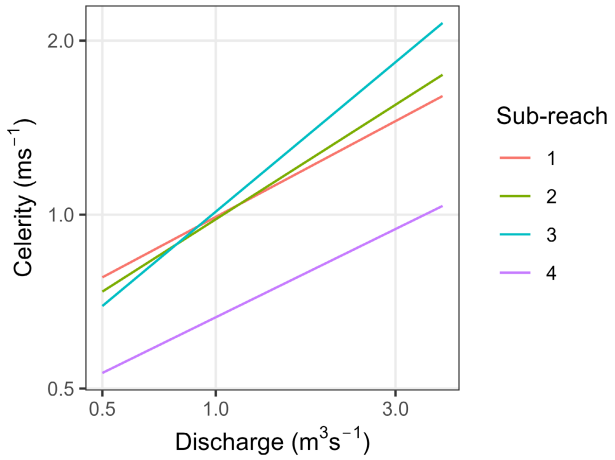

FIGURE 9 | Relationships between celerity and discharge based on Equation (17). Both axes are logarithmic.

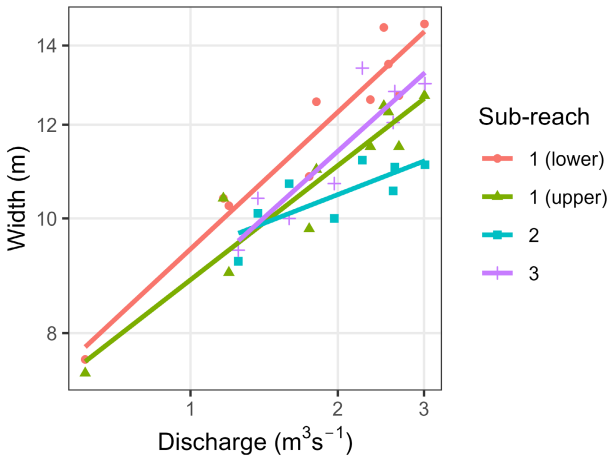

FIGURE 10 | Relationships between width and discharge (Q), showing the observed values and best-fit lines. Both axes are logarithmic.

TABLE 3 | Estimated parameters in the power-law relationship between width and discharge.

Sub-reach	a	b	n
1 (lower)	9.433	0.385	10
1 (upper)	8.886	0.321	10
2	9.378	0.161	8
3	8.816	0.373	8

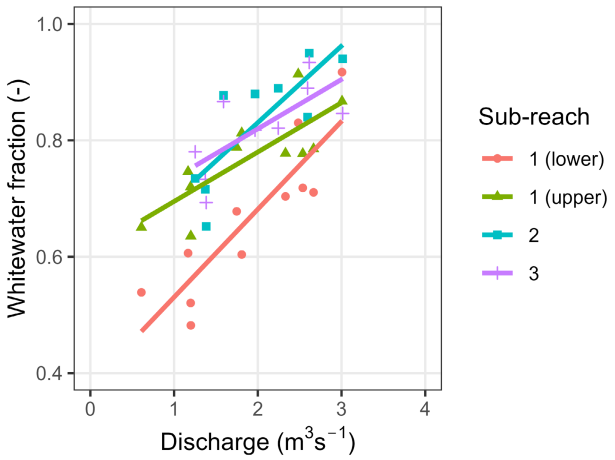

FIGURE 11 | Relationships between whitewater fractional coverage and discharge (Q), showing the observed values and best-fit lines. Both axes are linear.

TABLE 4 | Estimated parameters in the linear relationship between whitewater coverage and discharge.

Sub-reach	a_{ww}	b_{ww}	r^2	s_e	n	p
1 (lower)	0.380	0.151	0.78	0.066	8	<0.001
1 (upper)	0.610	0.085	0.63	0.053	8	0.004
2	0.567	0.132	0.65	0.067	8	0.009
3	0.650	0.085	0.52	0.056	8	0.028

Note: a_{ww} is the intercept and b_{ww} is the slope; r^2 is the coefficient of determination, s_e is the residual standard error, n is the number of data point used to fit the regression and p is the p-value for the regression.

Fractional whitewater coverage ranged from just under 0.5 up to 0.94 (Figure 11). It had a statistically significant linear relationship with discharge for all reaches covered by the drone flights (Table 4). For a given discharge, whitewater coverage was lowest for the most downstream reach, and similar for the other three reaches.

4 | Discussion

4.1 | Streamflow Variability

The 90% prediction limits shown in Figure 6 indicate an uncertainty of less than ±10% for discharges from about 1.3 to 3.5 $m^3 s^{-1}$, which is a typical level of accuracy for streamflow measurement by salt dilution in steep mountain streams (Richardson, Moore, and Zimmermann 2017). One potential source of error associated with grouping sub-reaches 1/2 and 3/4 for producing rating curves is related to the time taken for a discharge value to propagate from the pressure transducer to the bottoms of the measurement sub-reaches, which would generate a temporal mismatch between the observed discharge and the stage value with which it was paired. However, celerities computed based on the assumption of kinematic flow suggest that this temporal mismatch should be on the order of 8 min or less. A further consideration is the finding by Kellerhals (1969) that observed wave celerities in step-pool

channels were considerably greater than those based on kinematic flow. He attributed this finding to the fact that waves propagate at the dynamic celerity in pools, which is greater than the kinematic celerity. As a consequence, discharge values would propagate downstream more rapidly than our calculations based on kinematic flow, and errors in the rating curves due to not accounting for wave propagation lag times should be minor.

Differences in streamflow between sub-reaches 1/2 and 3/4 suggest that the study reach was initially gaining, with a gradual decline in the computed net inflow during a period of dry weather that led to losing conditions. An abrupt shift back to gaining flow coincided with a rain event. This pattern suggests that inflow occurred somewhere within sub-reach 2, upstream of the lower end of the salt dilution mixing reach. The decline in net inflow during the period of dry weather, estimated as $Q_{1/2} - Q_{3/4}$, would be consistent with a drop in the water table elevation and a shift from groundwater discharge into the stream to infiltration losses from the stream into the subsurface. The rainfall event on August 22–24 could have recharged the near-stream groundwater, resulting in a rise in the water table and a shift back to gaining conditions. However, these comments must be considered hypothetical given the lack of confirmatory observations regarding groundwater discharge or bed infiltration.

From the perspective of stream temperature modelling, the longitudinal variations in streamflow can be used to estimate the presence/absence and approximate magnitude of advective heat inputs. For example, flow losses along a channel by infiltration have no direct influence on water temperature apart from the indirect effects associated with downstream changes in velocity, width and depth. On the other hand, for periods with gaining flow, the advective heat input could be estimated from the longitudinal rate of increase in streamflow and an assumed range of inflow temperatures.

In addition to quantifying discharge and velocity, tracer BTC have been used to quantify bi-directional stream-subsurface water exchanges (e.g. Payn et al. 2009; Szeftel, Moore, and Weiler 2011), which can be important influences on stream temperature (e.g. Johnson 2004; King and Neilson 2019; Leach and Moore 2011). However, it should be noted that the information available for parameter determination in a BTC resulting from a slug injection is lower than that contained in its constant rate counterpart (Wagner and Harvey 1997). Unfortunately, it is logistically difficult to apply constant rate injection for higher discharges typical of proglacial streams during summer. In addition, it can be challenging to separate the effects of within-channel transient storage from hyporheic exchange (e.g. Neilson et al. 2010; Scordo and Moore 2009).

4.2 | Hydraulic Geometry

The approaches applied in this study made it possible to quantify hydraulic geometry relationships in a steep, complex channel with rapidly varying stream discharge, and should be feasible to apply for other steep proglacial channels as long as reaches with adequate lateral mixing exist. One caveat for the calculated velocities is that, when making streamflow measurements, the mixing reach for the salt dilution measurements only sampled the lower portion of each sub-reach, with points for injecting salt and monitoring tracer BTC chosen so as to provide complete lateral mixing and well-defined BTC. Hence, the velocity–discharge relationships may not represent conditions along the sub-reaches, in contrast to the width measurements, for which cross sections sampled each entire study reach. This mismatch could potentially influence the calculated celerities.

Analytical approaches to estimating hydraulic geometry equations assume that roughness remains constant at all flows, then derive the power-law relations for an assumed cross-sectional geometry. For example, Ferguson (1986) showed that triangular cross sections have a velocity exponent value of $m = 0.25$ and that parabolic cross sections have values of $m = 0.31$. The values of m for the study reaches are slightly greater than 0.31 for reaches 1 and 4 (0.32 and 0.35) and substantially greater for reaches 2 and 3 (0.42 and 0.54). Other studies have found that the velocity exponent in steep streams commonly averages about 0.5 (Comiti et al. 2007; David et al. 2010; Kellerhals 1969), and can be as high as 0.84 (Lee and Ferguson 2002). The width exponents predicted by Ferguson for idealised cross-sectional geometry range from 0.38 for triangular cross sections to 0.23 for parabolic cross sections. The width exponents in this study range from $b = 0.16$ to 0.38 are thus consistent with or smaller than Ferguson's results (Table 3).

4.3 | Whitewater Coverage and Implications for Stream Albedo and Stream Warming

As was hypothesised, there were statistically significant positive relationships between whitewater coverage and stream discharge. For the ranges of discharges sampled, these relationships could be modelled as linear functions. However, an asymptotic model would be required to extend the relationships to higher flows.

As seen in Figure 11, whitewater coverage generally exceeded 0.5 for the range of recorded flows, and exceeded 0.8 once flows reached $3\,m^3\,s^{-1}$. Based on results from McMahon and Moore (2017) and Richards and Moore (2011), the albedo of steep, aerated streams ranges from about 0.15 to 0.4, depending on incidence angle for direct solar radiation, atmospheric transmissivity, sediment concentration and discharge. In contrast, the albedo of flatwater streams in this mountainous region ranges from about 0.05 to 0.1 for low turbidity and up to 0.2 for higher turbidity (McMahon and Moore 2017). These results suggest that reach-averaged albedo could range from a low of 0.1 ($0.5 \times 0.15 + 0.5 \times 0.05$) for lower flows to around 0.36 ($0.8 \times 0.4 + 0.2 \times 0.2$) or even higher for full aeration. These values range higher than the values of 0.05–0.1 that have been used in previous efforts to model stream temperature in proglacial streams and rivers (Chikita et al. 2010; Magnusson, Jonas, and Kirchner 2012).

Solar radiation is typically the dominant energy input on summer days. For example, Magnusson, Jonas, and Kirchner (2012) reported that net solar radiation averaged $327\,W\,m^{-2}$ on summer days compared to an estimated total surface energy input of $411\,W\,m^{-2}$ (see their Table 2) based on an assumed albedo of 0.05. Using an albedo of 0.3 in the heat flux calculations would

reduce net solar radiation to 241 $W m^{-2}$ and net surface energy input to 325 $W m^{-2}$. Therefore, the effect of aeration on albedo could substantially reduce energy inputs by net solar radiation and thus reduce downstream warming for higher streamflow.

The results of this study and Richards and Moore (2011) suggest that albedo should be parameterised as an asymptotic function of stream discharge for steep channels and rapids. However, the current results suggest that model parameters vary amongst reaches, and further research on a broader range of streams should explore whether generalised relationships between whitewater coverage (or albedo) and stream discharge can be developed.

A further implication of the relationship between whitewater coverage and discharge is associated with the expected decline in summer stream discharge as glaciers in western North America continue to retreat (Frans et al. 2018; Jost et al. 2012). As outlined by Leach et al. (2023), downstream warming should increase with decreasing discharge due to reduced mean stream depth and reduced velocity, the latter of which would increase the time taken for water to flow through a reach and thus the opportunity for warming. In addition to these mechanisms, lower discharge would also be associated with lower albedo and thus greater absorption of solar radiation, which would further act to increase downstream warming rates.

5 | Conclusions

The combination of drone-based photogrammetry and streamflow measurements via salt dilution made it possible to quantify hydraulic geometry relationships for a steep, complex channel with rapidly varying flow. This approach holds promise for application at other steep proglacial streams, as long as sections with adequate lateral mixing occur within each reach. One qualification is that the computed velocities apply only to the reach between the salt injection point and the location at which the BTC is recorded.

Coverage of the water surface by whitewater for the subreaches had a significant positive relationship with discharge, which could be represented by a linear function for the range of flows captured by the drone photography. However, an asymptotic model would be required to extend the relationship to higher flows.

Whitewater generally covered over 50% of the water surface in all sub-reaches, and over 80% at the higher flows sampled. Consequently, the increase of albedo with increasing discharge would act to reduce energy inputs and thus downstream warming at higher flows, reinforcing the effects of increasing mean depth and velocity as discharge increases. As summer stream discharge declines as a result of glacier retreat, the resulting decrease in albedo would result in greater downstream warming rates, reinforcing the effects of decreasing mean depth and velocity.

Further research should apply these approaches to a broader range of streams to determine whether the coefficients in the hydraulic geometry and whitewater coverage–discharge relationships can be modelled as a function of slope, morphology or other channel characteristics. Such relationships would support the application of stream temperature models to assess the effects of climate change and glacier retreat on stream thermal regimes.

Acknowledgements

This research was conducted on the ancestral, traditional and unceded territory of the Stʼátʼimc First Nation. Financial support was provided by funds from a Natural Sciences and Engineering Research Council Discovery Grant held by RDM. ALD was also supported by a graduate award from the UBC Faculty of Arts. Jordyn Carss, Haley Williams, Stefan Gronsdahl, Johannes Exler, Martin Cermak, and Greg Wellage assisted with field work. We thank the two anonymous reviewers for thoughtful comments that helped us improve the manuscript.

Data Availability Statement

The data and scripts used to conduct the analyses are publicly available via https://zenodo.org/records/14210265.

References

Arismendi, I., M. Safeeq, J. B. Dunham, and S. L. Johnson. 2014. "Can Air Temperature Be Used to Project Influences of Climate Change on Stream Temperature?" *Environmental Research Letters* 9, no. 8: 084015. https://doi.org/10.1088/1748-9326/9/8/084015.

Baker, E. A., L. K. Lautz, C. A. Kelleher, and J. M. McKenzie. 2018. "The Importance of Incorporating Diurnally Fluctuating Stream Discharge in Stream Temperature Energy Balance Models." *Hydrological Processes* 32, no. 18: 2901–2914. https://doi.org/10.1002/hyp.13226.

Barbarossa, V., J. Bosmans, N. Wanders, et al. 2021. "Threats of Global Warming to the World's Freshwater Fishes." *Nature Communications* 12, no. 1: 1701. https://doi.org/10.1038/s41467-021-21655-w.

Bird, L. A., A. N. Moyer, R. D. Moore, and M. N. Koppes. 2022. "Hydrology and Thermal Regime of an Ice-Contact Proglacial Lake: Implications for Stream Temperature and Lake Evaporation." *Hydrological Processes* 36, no. 4: e14566. https://doi.org/10.1002/hyp.14566.

Boyd, M., and B. Kasper. 2003. "Analytical Methods for Dynamic Open Channel Heat and Mass Transfer: Methodology for the Heat Source Model Version 7.0." https://www.oregon.gov/deq/FilterDocs/heatsourcemanual.pdf.

Buahin, C. A., J. S. Horsburgh, and B. T. Neilson. 2019. "Parallel Multi-Objective Calibration of a Component-Based River Temperature Model." *Environmental Modelling & Software* 116: 57–71. https://doi.org/10.1016/j.envsoft.2019.02.012.

Caissie, D., M. G. Satish, and N. El-Jabi. 2007. "Predicting Water Temperatures Using a Deterministic Model: Application on Miramichi River Catchments (New Brunswick, Canada)." *Journal of Hydrology* 336, no. 3–4: 303–315. https://doi.org/10.1016/j.jhydrol.2007.01.008.

Cardenas, M. B., M. Doering, D. S. Rivas, C. Galdeano, B. T. Neilson, and C. T. Robinson. 2014. "Analysis of the Temperature Dynamics of a Proglacial River Using Time-Lapse Thermal Imaging and Energy Balance Modeling." *Journal of Hydrology* 519: 1963–1973. https://doi.org/10.1016/j.jhydrol.2014.09.079.

Chen, Y. D., R. F. Carsel, S. C. McCutcheon, and W. L. Nutter. 1998. "Stream Temperature Simulation of Forested Riparian Areas: I. Watershed-Scale Model Development." *Journal of Environmental Engineering* 124, no. 4: 304–315. https://doi.org/10.1061/(asce)0733-9372(1998)124:4(304).

Chikita, K. A., R. Kaminaga, I. Kudo, T. Wada, and Y. Kim. 2010. "Parameters Determining Water Temperature of a Proglacial Stream:

The Phelan Creek and the Gulkana Glacier, Alaska." *River Research and Applications* 26, no. 8: 995–1004. https://doi.org/10.1002/rra.1311.

Clarke, G. K. C., A. H. Jarosch, F. S. Anslow, V. Radić, and B. Menounos. 2015. "Projected Deglaciation of Western Canada in the Twenty-First Century." *Nature Geoscience* 8, no. 5: 372–377. https://doi.org/10.1038/ngeo2407.

Comiti, F., L. Mao, A. Wilcox, E. E. Wohl, and M. A. Lenzi. 2007. "Field-Derived Relationships for Flow Velocity and Resistance in High-Gradient Streams." *Journal of Hydrology* 340, no. 1–2: 48–62. https://doi.org/10.1016/j.jhydrol.2007.03.021.

David, G. C. L., E. Wohl, S. E. Yochum, and B. P. Bledsoe. 2010. "Controls on At-a-Station Hydraulic Geometry in Steep Headwater Streams, Colorado, USA." *Earth Surface Processes and Landforms* 35, no. 15: 1820–1837. https://doi.org/10.1002/esp.2023.

Dingman, S. L., and S. Afshari. 2018. "Field Verification of Analytical At-a-Station Hydraulic-Geometry Relations." *Journal of Hydrology* 564: 859–872. https://doi.org/10.1016/j.jhydrol.2018.07.020.

Duan, N. 1983. "Smearing Estimate: A Nonparametric Retransformation Method." *Journal of the American Statistical Association* 78, no. 383: 605–610. https://doi.org/10.1080/01621459.1983.10478017.

Dugdale, S. J., D. M. Hannah, and I. A. Malcolm. 2017. "River Temperature Modelling: A Review of Process-Based Approaches and Future Directions." *Earth-Science Reviews* 175: 97–113. https://doi.org/10.1016/j.earscirev.2017.10.009.

Dugdale, S. J., C. A. Kelleher, I. A. Malcolm, S. Caldwell, and D. M. Hannah. 2019. "Assessing the Potential of Drone-Based Thermal Infrared Imagery for Quantifying River Temperature Heterogeneity." *Hydrological Processes* 33, no. 7: 1152–1163. https://doi.org/10.1002/hyp.13395.

Dugdale, S. J., I. A. Malcolm, and D. M. Hannah. 2019. "Drone-Based Structure-From-Motion Provides Accurate Forest Canopy Data to Assess Shading Effects in River Temperature Models." *Science of the Total Environment* 678: 326–340. https://doi.org/10.1016/j.scitotenv.2019.04.229.

Dugdale, S. J., I. A. Malcolm, K. Kantola, and D. M. Hannah. 2018. "Stream Temperature Under Contrasting Riparian Forest Cover: Understanding Thermal Dynamics and Heat Exchange Processes." *Science of the Total Environment* 610-611: 1375–1389. https://doi.org/10.1016/j.scitotenv.2017.08.198.

Eaton, J. G., and R. M. Scheller. 1996. "Effects of Climate Warming on Fish Thermal Habitat in Streams of the United States." *Limnology and Oceanography* 41, no. 5: 1109–1115. https://doi.org/10.4319/lo.1996.41.5.1109.

Ferguson, R. 2007. "Flow Resistance Equations for Gravel- and Boulder-Bed Streams." *Water Resources Research* 43, no. 5: 1–12. https://doi.org/10.1029/2006wr005422.

Ferguson, R. I. 1986. "Hydraulics and Hydraulic Geometry." *Progress in Physical Geography: Earth and Environment* 10, no. 1: 1–31. https://doi.org/10.1177/030913338601000101.

Fleming, S. W. 2005. "Comparative Analysis of Glacial and Nival Streamflow Regimes With Implications for Lotic Habitat Quantity and Fish Species Richness." *River Research and Applications* 21, no. 4: 363–379. https://doi.org/10.1002/rra.810.

Foreman, M. G. G., C. B. James, M. C. Quick, P. Hollemans, and E. Wiebe. 1997. "Flow and Temperature Models for the Fraser and Thompson Rivers." *Atmosphere-Ocean* 35, no. 1: 109–134. https://doi.org/10.1080/07055900.1997.9649587.

Frans, C., E. Istanbulluoglu, D. P. Lettenmaier, A. G. Fountain, and J. Riedel. 2018. "Glacier Recession and the Response of Summer Streamflow in the Pacific Northwest United States, 1960–2099." *Water Resources Research* 54, no. 9: 6202–6225. https://doi.org/10.1029/2017wr021764.

Fuller, M. R., J. L. Ebersole, N. E. Detenbeck, R. Labiosa, P. Leinenbach, and C. E. Torgersen. 2021. "Integrating Thermal Infrared Stream Temperature Imagery and Spatial Stream Network Models to Understand Natural Spatial Thermal Variability in Streams." *Journal of Thermal Biology* 100: 103028. https://doi.org/10.1016/j.jtherbio.2021.103028.

Fullerton, A. H., N. Sun, M. J. Baerwalde, B. L. Hawkins, and H. Yan. 2022. "Mechanistic Simulations Suggest Riparian Restoration Can Partly Counteract Climate Impacts to Juvenile Salmon." *JAWRA Journal of the American Water Resources Association* 58, no. 4: 525–546. https://doi.org/10.1111/1752-1688.13011.

Garner, G., I. A. Malcolm, J. P. Sadler, and D. M. Hannah. 2014. "What Causes Cooling Water Temperature Gradients in a Forested Stream Reach?" *Hydrology and Earth System Sciences* 18, no. 12: 5361–5376. https://doi.org/10.5194/hess-18-5361-2014.

Glose, A., L. K. Lautz, and E. A. Baker. 2017. "Stream Heat Budget Modeling With HFLUX: Model Development, Evaluation, and Applications Across Contrasting Sites and Seasons." *Environmental Modelling & Software* 92: 213–228. https://doi.org/10.1016/j.envsoft.2017.02.021.

Greenwell, B. M., and C. M. S. Kabban. 2014. "Investr: An R Package for Inverse Estimation." *R Journal* 6: 90–100. https://doi.org/10.32614/RJ-2014-009.

Gu, R. 1998. "A Rating-Curve Method for Hydrodynamic Simulations in Contaminant Transport Modeling." *JAWRA Journal of the American Water Resources Association* 34, no. 2: 397–407. https://doi.org/10.1111/j.1752-1688.1998.tb04144.x.

Huss, M., and R. Hock. 2018. "Global-Scale Hydrological Response to Future Glacier Mass Loss." *Nature Climate Change* 8, no. 2: 135–140. https://doi.org/10.1038/s41558-017-0049-x.

Iacarella, J. C., R. Chea, D. A. Patterson, and J. D. Weller. 2024. "Projecting Exceedance of Juvenile Salmonid Thermal Maxima in Streams Under Climate Change: A Crosswalk From Lab Experiments to Riparian Restoration." *Freshwater Biology* 69, no. 9: 1218–1231. https://doi.org/10.1111/fwb.14300.

Javernick, L., J. Brasington, and B. Caruso. 2014. "Modeling the Topography of Shallow Braided Rivers Using Structure-From-Motion Photogrammetry." *Geomorphology* 213: 166–182. https://doi.org/10.1016/j.geomorph.2014.01.006.

Johnson, M. F., L. K. Albertson, A. C. Algar, et al. 2024. "Rising Water Temperature in Rivers: Ecological Impacts and Future Resilience." *WIREs Water* 11, no. 4: e1724. https://doi.org/10.1002/wat2.1724.

Johnson, S. L. 2004. "Factors Influencing Stream Temperatures in Small Streams: Substrate Effects and a Shading Experiment." *Canadian Journal of Fisheries and Aquatic Sciences* 61, no. 6: 913–923. https://doi.org/10.1139/f04-040.

Jost, G., R. D. Moore, B. Menounos, and R. Wheate. 2012. "Quantifying the Contribution of Glacier Runoff to Streamflow in the Upper Columbia River Basin, Canada." *Hydrology and Earth System Sciences* 16, no. 3: 849–860. https://doi.org/10.5194/hess-16-849-2012.

Kellerhals, R. 1969. "Runoff Concentration in Steep Channel Networks." PhD thesis, University of British Columbia. https://open.library.ubc.ca/media/download/pdf/831/1.0093330/1.

Khamis, K., L. E. Brown, A. M. Milner, and D. M. Hannah. 2015. "Heat Exchange Processes and Thermal Dynamics of a Glacier-Fed Alpine Stream." *Hydrological Processes* 29, no. 15: 3306–3317. https://doi.org/10.1002/hyp.10433.

King, T. V., and B. T. Neilson. 2019. "Quantifying Reach-Average Effects of Hyporheic Exchange on Arctic River Temperatures in an Area of Continuous Permafrost." *Water Resources Research* 55, no. 3: 1951–1971. https://doi.org/10.1029/2018wr023463.

Leach, J. A., C. Kelleher, B. L. Kurylyk, R. D. Moore, and B. T. Neilson. 2023. "A Primer on Stream Temperature Processes." *WIREs Water* 10, no. 4: e1643. https://doi.org/10.1002/wat2.1643.

Leach, J. A., and R. D. Moore. 2010. "Above-Stream Microclimate and Stream Surface Energy Exchanges in a Wildfire-Disturbed Riparian Zone." *Hydrological Processes* 24, no. 17: 2369–2381. https://doi.org/10.1002/hyp.7639.

Leach, J. A., and R. D. Moore. 2011. "Stream Temperature Dynamics in Two Hydrogeomorphically Distinct Reaches." *Hydrological Processes* 25, no. 5: 679–690. https://doi.org/10.1002/hyp.7854.

Leach, J. A., and R. D. Moore. 2019. "Empirical Stream Thermal Sensitivities May Underestimate Stream Temperature Response to Climate Warming." *Water Resources Research* 55: 5453–5467. https://doi.org/10.1029/2018WR024236.

Lee, A. J., and R. I. Ferguson. 2002. "Velocity and Flow Resistance in Step-Pool Streams." *Geomorphology* 46, no. 1–2: 59–71. https://doi.org/10.1016/s0169-555x(02)00054-5.

Leopold, L. B., and T. Maddock. 1953. *The Hydraulic Geometry of Stream Channels and Some Physiographic Implications. Professional Paper No. 252*. Washington, DC: United States Geological Survey; US Government Printing Office.

MacDonald, R. J., S. Boon, and J. M. Byrne. 2014. "A Process-Based Stream Temperature Modelling Approach for Mountain Regions." *Journal of Hydrology* 511: 920–931. https://doi.org/10.1016/j.jhydrol.2014.02.009.

Magnusson, J., T. Jonas, and J. W. Kirchner. 2012. "Temperature Dynamics of a Proglacial Stream: Identifying Dominant Energy Balance Components and Inferring Spatially Integrated Hydraulic Geometry." *Water Resources Research* 48, no. 6: 1–16. https://doi.org/10.1029/2011wr011378.

McMahon, A., and R. D. Moore. 2017. "Influence of Turbidity and Aeration on the Albedo of Mountain Streams." *Hydrological Processes* 31: 4477–4491. https://doi.org/10.1002/hyp.11370.

McParland, D., B. Eaton, and J. Rosenfeld. 2014. "At-a-Station Hydraulic Geometry Simulator." *River Research and Applications* 32, no. 3: 399–410. https://doi.org/10.1002/rra.2851.

Meier, W., C. Bonjour, A. Wüest, and P. Reichert. 2003. "Modeling the Effect of Water Diversion on the Temperature of Mountain Streams." *Journal of Environmental Engineering* 129, no. 8: 755–764. https://doi.org/10.1061/(asce)0733-9372(2003)129:8(755).

Moore, R. D. 2024. "Fitting Power-Law Relations in Watershed Science and Analysis, With an Example Using the R Language." *Confluence: Journal of Watershed Science and Management* 7, no. 1: 1–14. https://doi.org/10.22230/jwsm.2024v7n1a53.

Moore, R. D., S. W. Fleming, B. Menounos, et al. 2009. "Glacier Change in Western North America: Influences on Hydrology, Geomorphic Hazards and Water Quality." *Hydrological Processes* 23, no. 1: 42–61. https://doi.org/10.1002/hyp.7162.

Moore, R. D., D. Spittlehouse, P. Whitfield, and K. Stahl. 2010. "Weather and Climate." In *Compendium of Forest Hydrology and Geomorphology in British Columbia*, edited by R. Pike, T. E. Redding, R. D. Moore, R. D. Winkler, and K. D. Bladon, 47–84. Victoria, British Columbia: Province of British Columbia. https://a100.gov.bc.ca/pub/eirs/finishDownloadDocument.do?subdocumentId=12552.

Moore, R. D., P. Sutherland, T. Gomi, and A. Dhakal. 2005. "Thermal Regime of a Headwater Stream Within a Clear-Cut, Coastal British Columbia, Canada." *Hydrological Processes* 19, no. 13: 2591–2608. https://doi.org/10.1002/hyp.5733.

Neilson, B. T., D. K. Stevens, S. C. Chapra, and C. Bandaragoda. 2010. "Two-Zone Transient Storage Modeling Using Temperature and Solute Data With Multiobjective Calibration: 2. Temperature and Solute." *Water Resources Research* 46, no. 12: W12520. https://doi.org/10.1029/2009wr008759.

Nelitz, M. A., E. A. MacIsaac, and R. M. Peterman. 2007. "A Science-Based Approach for Identifying Temperature-Sensitive Streams for Rainbow Trout." *North American Journal of Fisheries Management* 27, no. 2: 405–424. https://doi.org/10.1577/m05-146.1.

Parkinson, E. A., E. V. Lea, M. A. Nelitz, J. M. Knudson, and R. D. Moore. 2016. "Identifying Temperature Thresholds Associated With Fish Community Changes in British Columbia, Canada, to Support Identification of Temperature Sensitive Streams." *River Research and Applications* 32: 330–347. https://doi.org/10.1002/rra.2867.

Payn, R. A., M. N. Gooseff, B. L. McGlynn, K. E. Bencala, and S. M. Wondzell. 2009. "Channel Water Balance and Exchange With Subsurface Flow Along a Mountain Headwater Stream in Montana, United States." *Water Resources Research* 45, no. 11: W11427. https://doi.org/10.1029/2008wr007644.

Pitman, K. J., and J. W. Moore. 2021. "The Role of Large, Glaciated Tributaries in Cooling an Important Pacific Salmon Migration Corridor: A Study of the Babine River." *Environmental Biology of Fishes* 104, no. 10: 1263–1277. https://doi.org/10.1007/s10641-021-01152-1.

Richards, J., and R. D. Moore. 2011. "Discharge Dependence of Stream Albedo in a Steep Proglacial Channel." *Hydrological Processes* 25, no. 26: 4154–4158. https://doi.org/10.1002/hyp.8343.

Richardson, M., R. D. Moore, and A. Zimmermann. 2017. "Variability of Tracer Breakthrough Curves in Mountain Streams: Implications for Streamflow Measurement by Slug Injection." *Canadian Water Resources Journal / Revue Canadienne Des Ressources Hydriques* 42, no. 1: 21–37. https://doi.org/10.1080/07011784.2016.1212676.

Richardson, M., G. Sentlinger, R. D. Moore, and A. Zimmermann. 2017. "Quantifying the Relation Between Electrical Conductivity and Salt Concentration for Dilution Gauging via Dry Salt Injection." *Confluence: Journal of Watershed Science and Management* 1, no. 2: 1–14. https://doi.org/10.22230/jwsm.2017v1n2a1.

Ryder, J. M. 1991. "Geomorphological Processes Associated With an Ice-Marginal Lake at Bridge Glacier, British Columbia." *Géographie Physique et Quaternaire* 45, no. 1: 35–44. https://doi.org/10.7202/032843ar.

Saraeva, E., and T. B. Hardy. 2009. "Prediction of Fisheries Physical Habitat Values Based on Hydraulic Geometry and Frequency Distributions of Depth and Velocity." *International Journal of River Basin Management* 7, no. 1: 31–41. https://doi.org/10.1080/15715124.2009.9635368.

Schneider, J. M., D. Rickenmann, J. M. Turowski, and J. W. Kirchner. 2015. "Self-Adjustment of Stream Bed Roughness and Flow Velocity in a Steep Mountain Channel." *Water Resources Research* 51, no. 10: 7838–7859. https://doi.org/10.1002/2015wr016934.

Scordo, E. B., and R. D. Moore. 2009. "Transient Storage Processes in a Steep Headwater Stream." *Hydrological Processes* 23, no. 18: 2671–2685. https://doi.org/10.1002/hyp.7345.

St-Hilaire, A., G. Morin, N. El-Jabi, and D. Caissie. 2000. "Water Temperature Modelling in a Small Forested Stream: Implication of Forest Canopy and Soil Temperature." *Canadian Journal of Civil Engineering* 27, no. 6: 1095–1108. https://doi.org/10.1139/l00-021.

Sun, N., J. Yearsley, N. Voisin, and D. P. Lettenmaier. 2015. "A Spatially Distributed Model for the Assessment of Land Use Impacts on Stream Temperature in Small Urban Watersheds." *Hydrological Processes* 29, no. 10: 2331–2345. https://doi.org/10.1002/hyp.10363.

Szeftel, P., R. D. Moore, and M. Weiler. 2011. "Influence of Distributed Flow Losses and Gains on the Estimation of Transient Storage Parameters From Stream Tracer Experiments." *Journal of Hydrology* 396, no. 3–4: 277–291. https://doi.org/10.1016/j.jhydrol.2010.11.018.

Szeitz, A. J., and R. D. Moore. 2020. "Predicting Evaporation From Mountain Streams." *Hydrological Processes* 34, no. 22: 4262–4279. https://doi.org/10.1002/hyp.13875.

van Vliet, M. T. H., J. R. Yearsley, W. H. P. Franssen, et al. 2012. "Coupled Daily Streamflow and Water Temperature Modelling in Large River

Basins." *Hydrology and Earth System Sciences* 16, no. 11: 4303–4321. https://doi.org/10.5194/hess-16-4303-2012.

Wagner, B. J., and J. W. Harvey. 1997. "Experimental Design for Estimating Parameters of Rate-Limited Mass Transfer: Analysis of Stream Tracer Studies." *Water Resources Research* 33, no. 7: 1731–1741. https://doi.org/10.1029/97wr01067.

Weller, J. D., R. D. Moore, and J. C. Iacarella. 2023. "Stream Thermalscape Scenarios for British Columbia, Canada." *Canadian Water Resources Journal / Revue Canadienne Des Ressources Hydriques* 49, no. 2: 233–252. https://doi.org/10.1080/07011784.2023.2267028.

Yearsley, J. R. 2009. "A Semi-Lagrangian Water Temperature Model for Advection-Dominated River Systems." *Water Resources Research* 45, no. 12: W12405. https://doi.org/10.1029/2008wr007629.

Zemp, M., M. Huss, E. Thibert, et al. 2019. "Global Glacier Mass Changes and Their Contributions to Sea-Level Rise From 1961 to 2016." *Nature* 568, no. 7752: 382–386. https://doi.org/10.1038/s41586-019-1071-0.

Zimmermann, A. 2010. "Flow Resistance in Steep Streams: An Experimental Study." *Water Resources Research* 46, no. 9: 1–18. https://doi.org/10.1029/2009wr007913.